Published in final edited form as:
J Comp Neurol. 2006 February 10; 494(5): 738–751. doi:10.1002/cne.20841.

A Developmental Period for NMDA Receptor-Dependent Synapse Elimination Correlated with Visuotopic Map Refinement

Matthew T. Colonnese[*] and **Martha Constantine-Paton**
McGovern Institute for Brain Research, Departments of Biology and Brain and Cognitive, Sciences, Massachusetts Institute of Technology, 77 Massachusetts Avenue, Bldg 68-380, Cambridge, Massachusetts 02139-4307

Abstract

During a short perinatal interval, NMDA receptor (NMDAR) function is essential to a process in which spontaneous retinal waves focus retinal axon arbors in the superficial layers of the rodent superior colliculus (sSC). Here we provide evidence that this NMDAR-dependent axonal refinement occurs through elimination of un-correlated retinal synapses arising from disparate loci, rather than stabilization of topographically-appropriate inputs. The density of synaptic release sites within fluorescently labeled retinal terminals was counted in double labeling experiments using confocal microscopy and antibodies against synaptophysin or synapsin-1. Chronic NMDAR blockade from birth increased retinal axon synapse density at postnatal days (P) 6, 8 and 10, suggesting that NMDAR currents reduce synapse density during the refinement period. When assayed at P14, after focal arborization has been established, the effect disappeared. Conversely, chronic NMDA treatment, known to induce functional synaptic depression in the sSC, decreased retinocollicular synapse density at P14, but not earlier, during the refinement period (P8). Thus during the development of retinocollicular topographic order, there is a period when NMDAR activity predominantly eliminates retinal axon synapses. We were able to extend this period by using retinal lesions to reduce synaptic density in a defined zone. Synapse density on intact retinocollicular axons sprouting into this zone was increased by NMDAR blockade, even when examined at P14. Thus, the period of NMDAR-dependent synaptic destabilization is terminated by a factor related to the density and refinement of retinal arbors.

Keywords

superior colliculus; rat; spontaneous activity; plasticity; eye opening

Retinal ganglion cell (RGC) axons form a topographic projection in the superficial layers of the superior colliculus (sSC) using cell surface cues that establish gross orientation (Feldheim et al., 2000), and patterned “spontaneous” RGC activity that refines the point to point ordering of the axons into small, topographically ordered arbors (McLaughlin et al., 2003). The removal of retinal axon terminals from ectopic locales during this refinement process requires NMDA receptor (NMDAR) activity (Simon et al., 1992; Huang and Pallas, 2001). NMDARs are hypothesized to drive this and other developmental instances of refinement by selectively stabilizing correlated inputs as a result of a persistent long-term potentiation of synaptic strength (Constantine-Paton et al., 1990), and/or by actively destabilizing those inputs that become functionally depressed as a result of poorly correlated activity (Stent, 1973; Abraham and Bear, 1996). However, experiments that distinguish the

Correspondence to: Dr. Matthew T. Colonnese, Phone: (617) 258-0467, Fax: (617), email: mcolonne@mit.edu.
Associate Editor: Leslie P. Tolbert

relative contributions of these two processes during refinement *in vivo* have not been performed.

We examined synapse formation by RGC axons in sSC during and after the period of axon terminal refinement. The emergence of dense, topographically appropriate retinal axon terminal arbors occurs in the rat sSC between post-natal day (P)4 and P12 by the exuberant elaboration of arbors, and their elimination from incorrect regions (Simon and O'Leary, 1992). Retinal axons can develop gross topographic order in the absence of retinal activity (O'Leary and Cowan, 1983), through positional cues provided by gradients of membrane bound guidance molecules (O'Leary et al., 1999). However, correlated RGC activity is also necessary for refinement of the retinal axon arbors into focused terminations. This activity is provided by spontaneous waves of depolarization driven by cholinergic retinal amacrine cells (Feller et al., 1996), and later through glutamatergic synapses (Wong et al., 2000). The early cholinergic waves appear particularly important. β2 cholinergic receptor knockout mice do not have these waves, though their RGCs are still spontaneously active. These animals develop axon arbors that are more dispersed and less dense than wild type (Bansal et al., 2000; McLaughlin et al., 2003). The ectopic terminals of these mice remain even after normal photoreceptor driven activity develops (~P8–P11).

NMDAR blockade also prevents the removal of ectopic retinal arbors from topographically inappropriate locales in the developing sSC (Simon et al., 1992), although the development of clumped ipsilateral axons restricted to the stratum opticum is not disrupted (Colonnese and Constantine-Paton, 2001). NMDAR currents are normally down-regulated by increases in retinal activity coincident with the end of retinotopic map refinement (Shi et al., 1997; Shi et al., 2000; Townsend et al., 2004), suggesting that this regulation of the NMDAR current may play a role in the termination of the period for topographic mapping.

Studies in some systems have suggested that initial synapse formation is a trial and error process in which the NMDAR is one of the primary determinants of synaptic stability (Rajan et al., 1999b), while other systems have indicated that the receptor can also be a determinant of synaptic elimination (Schmidt et al., 2000). To discriminate among these possibilities as the basis of the NMDAR-dependent refinement in the sSC, we have here quantitatively examined retinocollicular synapse density following chronic NMDAR antagonist or agonist treatment during, and shortly after, the period of topographic refinement. If NMDAR-dependent refinement is predominantly a result of stabilizing synapses, blockade of the receptor should decrease retinal terminal synapse density; conversely, if early NMDAR activation is primarily destabilizing synapses, blockade should increase retinal terminal synapse density. These experiments incorporate the assumption that synaptic weakening and destabilization leads to synapse loss. This can be tested using the agonist treatment. Chronic NMDA treatment induces synaptic depression in the sSC (Shi et al., 2001; Zhao and Constantine-Paton, 2002). Consequently, if functional depression is associated with a loss of synapses, this treatment should decrease retinal terminal synapse density.

We have previously used lesion-induced sprouting of the ipsilateral projection to provide information on the relationship between NMDAR activity, synapse elimination, and competition (Colonnese and Contantine-Paton, 2001; Colonnese and Constantine-Paton, 2005). On these axons NMDAR activity is clearly associated with synapse elimination and a reduction in sprouting. However the relevance of the sprouting ipsilateral projection to normal development is not known. Therefore, in the present set of experiments we examined the refining contralateral projection to ask whether elimination of synaptic contacts predominates during the normal development of retinocollicular topographic order, as suggested by the earlier studies.

METHODS

Animals and materials

All procedures were approved by the MIT Committee on Animal Care. Timed pregnant Sprague-Dawley rats were acquired from Taconic Animal Labs (Germantown, NY) and housed in a 12/12hr light/dark cycle. The inert ethylene-vinyl acetate copolymer Elvax-40W (Dupont) was prepared with 2-amino-5-phosphonopentanoic acid (AP5) as previously reported (Cline and Constantine-Paton, 1989; Smith et al., 1995; Colonnese and Constantine-Paton, 2001; Colonnese et al., 2003), or with NMDA as previously reported (Aamodt et al., 2000; Shi et al., 2001). Control Elvax for antagonist experiments contained only the inactive isomer L-AP5; for the NMDA experiments sham Elvax was made-up with the vehicle, water that evaporated during subsequent production steps. We have previously estimated (Colonnese and Constantine-Paton, 2001) that concentrations of D-AP5 in the sSC to be above 20μM at all times, and in the 100μM range during the first few days after implantation. The concentration of NMDA is estimated to be above 5μM at all times, and in the 20μM range for the first few days after implantation. Litters were culled to 10 and equal numbers of pups in each litter received either active drug or control Elvax, so each treatment had littermate controls. Two litters for each group were included in the final analysis. The initiation times for chronic treatment varied slightly. AP5 treatment was begun at P0 in order to be the same treatment as has been previously characterized (Simon et al., 1992; Colonnese and Constantine-Paton, 2001; Colonnese et al., 2003). NMDA treatment could not be begun until P2 because earlier implantations resulted in high mortality of the pups. For the later time point, NMDA treatment was initiated at P8 in order to replicate the treatment that has been previously described (Aamodt et al., 2000; Shi et al., 2001; Zhao and Constantine-Paton, 2002).

Surgery

A lidocaine (2.5%) and prilocaine (2.5%) cream (Emla Cream Astra Pharmaceuticals) was applied to the skin or eye before all incisions to reduce post-operative pain. Elvax sections were implanted on various days using the method of Simon *et al.* (1992): under anesthesia, the scalp and skull were retracted, and the Elvax slab was positioned over the sSC, the front edge tucked under the occipital cortex. Anesthesia was provided by inhaled 1–2% isoflurane (1-chloro-2,2,2-trifluoroethyl difluoromethyl ether). A surgical plane of anesthesia was confirmed by a lack of response to toe pinch, and monitoring for rapid increases in breathing rate. Sutures and tissue adhesive (Vetbond, 3M Animal Care Products; St. Paul, MN) were used to close the incision. For eye lesions, pups were anesthetized and the left eyelid was opened with blunted iris scissors. The eyelids were retracted manually and the lesion was made by insertion of a #11 scalpel blade through the sclera, severing the axons of retinal ganglion cell axons lying at the temporal pole dorsal to the incision located approximately 2mm from the ciliary margin. For anterograde tracing of the contralateral retina, the cholera toxin B subunit (CTB) conjugated to Alexa 488 dye was used (Molecular Probes; Eugene, OR). Retinocollicular projections were labeled one (for P6 animals) or two (for P8 – P14 animals) days before sacrifice. Pups were anesthetized and a small hole was made in the cornea with a 28 gauge needle. Five μl of a solution of 0.2% CTB, 1% dimethyl-sulfoxide in PBS was then injected into the vitreous using a 31 gauge Hamilton syringe. The eye-lids were closed with Vetbond. The tracer was injected through the cornea to avoid further damage to retina that might result in a lesion of the retinal axons.

Pups were anesthetized with 3% isoflurane and killed by transcardial perfusion of PBS followed by 4% paraformaldehyde in 0.1M phosphate buffer, pH 7.2. The midbrain was removed and post-fixed overnight at 4°C. Animals with misplaced Elvax or damage to the sSC were excluded from further analysis (n=9 of 100). The midbrain was photographed in

whole mount epifluorescence to visualize the dorsal midbrain optic targets. The size of the scotoma was determined as a percentage of the area occupied by the collicular lobe in the micrographs. Brains with a lightly or incompletely labeled retinal projection were discarded (n=12 of 100). Nine pups died before sacrifice, for a total inclusion of 70 pups from 10 litters in the final analysis. In pups that received retinal lesions, previous work has revealed that deafferented regions (scotomas) occupying between 7% and 35% of the sSC show no significant correlation between their size and density of axons sprouting into them (Colonnese and Constantine-Paton, 2001). Therefore brains with scotomas outside this range were also discarded (n=4 of 30).

Immunohistochemistry

The antibodies used for immunohistochemistry were as follows. Synaptophysin: mouse monoclonal from Sigma-Aldrich (clone SVP-38, Cat# S5768, Lot# 098H4886); Synapsin-1: mouse monoclonal against the C-terminal region of sheep synapsin-1 (Chemicon International, Temecula, CA, Cat# MAB355, Lot# 22050107); GAD 65/67: rabbit IgG fraction against the KLH coupled synthetic peptide KDIDFLIEEIERLGQDL corresponding to the C-terminal region of human GAD-67 (Sigma-Aldrich, Cat# G5163, Lot# 028H4850); GluR1: rabbit affinity purified polyclonal against the rat carboxy terminus peptide SHSSGMPLGATGL conjugated to BSA with glutaraldehyde (Chemicon, Cat# AB1504, Lot# 20070481); GluR2: rabbit affinity purified polyclonal antibody against synthetic peptide VAKNPQNINPSSSQNS (rat GluR2 amino acids 827–842) cystine conjugated to BSA (Chemicon, Cat# AB1768; Lot# 20100973). All antibodies recognized a single band (or the expected doublet for GAD 65/67) by western blot of whole lysate P14 sSC (Fig. 1). The details of our western blotting methods have been previously published (Colonnese et al., 2003). For control of secondary antibody specificity, sections in which the primary antibody was excluded were processed for all antibodies. In all cases only dim autofluorescence was observed, with no signal similar to that observed with the primary antibody. Preadsorbtion controls were performed for the three polyclonal antibodies using the synthetic peptides against which they were raised. In all cases overnight preadsorbtion with a 10 fold excess of peptide prevented all cell body and punctate staining in P14 sSC, leaving only background staining similar to that seen following secondary antibody application alone.

All immunohistochemistry was performed in single batches for an entire litter; all imaging was completed within 2 days for each litter and all quantitative comparisons of synapse density were made within a litter. Midbrain blocks were embedded in 3.5% low melting point agarose and 8% sucrose in PBS and cut in coronal section ~30μm thick on a vibratome. Sections were pre-incubated for 1hr in 0.5% Triton X-100/ 4% serum in phosphate buffered saline (PBS), and then in the same solution plus primary antibody (synaptophysin, 6 μg/mL; synapsin-1, 2 μg/mL; GAD 65/67,14 μg/ml) overnight at 4°C. For double labeling of synaptophysin and GluR1 or GluR2 (both 2 μg/mL), no Triton X-100 was added during antibody incubation. Fluorescently labeled (Donkey anti-mouse conjugated to Cy5 (715-175-150, Jackson Laboratories, West Grove PA; or goat anti-mouse Alexa 633 (A21226) and goat anti-rabbit Alexa 546 (A11010, Molecular Probes) secondary antibodies were used for visualization after mounting on glass slides in an aqueous, hardening mounting media (Fluoromount, EM Sciences).

Microscopy

Laser-scanning confocal microscopy was performed on a Nikon PCM 2000 controlled by the Compix software package running on a Pentium based PC. For high-resolution images of synaptic puncta, a 60x, 1.40 NA objective was used to acquire images with a pixel size of $0.01\mu m^2$ in plane, and approximately 0.30 μm out of plane. Laser power, gain and black

level were carefully modulated to remove any fluorophore bleed-though between channels. These parameters were kept constant for a complete experiment that included all control and experimental pups in a litter. Within litters, the imaging of pups from each treatment group was interdigitated to reduce any effects of a slow shift in laser alignment or power. The specific group identity was coded so all microscopy and computer analysis was performed blind to treatment group.

Synaptic Analysis

Two 50 μm thick vibratome sections were cut at 500 μm and 600 μm from the rostral pole of each colliculus. Two regions from the center of each section (Fig. 2) were imaged. For the analysis of synaptic density in lesioned animals the scotoma was identified under low power, and the two regions were selected in the center of the scotoma. The sections analyzed were always within 400 – 600 μm of the **colliculus's** rostral edge; the selected regions were randomly chosen but lay at least 500 μm from either the medial or lateral edge of the sSC. For all sections the selected region was completely within the *stratum griseum superficiale* and *stratum zonale*. The dorsal edge of each region was 10 μm from the pial surface. Within each region, a stack of confocal images at intervals of 0.25μm was taken through a 102 × 102 × 4 μm volume of tissue. The first image was 4 μm from the cut surface of the slice. Single voxels were 0.1 × 0.1 μm in plane (x–y) and an estimated 0.30 μm out of plane (z). The depth of these volumes was selected to be superficial enough to contain constant and bright synaptophysin label, but to be deep enough that artifacts from the cut surface of the slice were not visible.

Image analysis was performed using the public domain NIH Image program (developed at the U.S. National Institutes of Health and available on the Internet at http://rsb.info.nih.gov/nih-image/).

The basic design of the synaptic analysis was to count, using an optical disector method (Gundersen, 1986), instances of overlap of retinal terminals and synaptic stain that met a minimum size criterion (see below). For noise reduction, a 3×3 pixel, low-pass filter was applied to each image. For analysis of the synaptic immunostain, a linear histogram stretch to normalize the brightest and darkest pixels in each image was applied to each section to enhance contrast. This equalized intensity differences due to tissue depth and photobleaching. The stretch was never greater than 30%. A threshold value was determined by visual examination of a number of micrographs from different animals within the litter to determine the intensity of in-focus fluorescence vs. background and out of focus fluorescence. A threshold of 4 standard deviations above the median intensity of the sections in a volume produced reliable exclusion of background. This median intensity was largely a result of autofluorescence, and did not change significantly with treatment. For axon terminals, which were more clearly separable from background, and showed no change in intensity from depth or bleaching, a threshold of five standard deviations above baseline was chosen after examination of multiple sections. An example of a counting field is shown in Figure 1b. A blowup of small region of this confocal section with normal contrast is shown in Figure 1c. The same region is shown after contrast enhancement and thresholding in Figure 1d.

In the contralateral retinocollicular projection axon arborization is extremely dense and small caliber terminal branches have tortuous trajectories rendering it difficult to reconstruct individual branches over long distances despite confocal reconstructions. Consequently, for quantification, the number of pixels containing above threshold retinal axon label and above threshold synaptic vesicle immunofluorescence were counted in each z-section. The values from each section in a volume were added together to obtain the density of retinal axons and vesicle label within that volume of neuropil. In addition, for each z-section, an image that

showed only the pixels occupied by both above threshold retinal terminals and above threshold synaptic stain was generated. The number of such pixels in each section was added together to generate a total number of "overlapped pixels" for each sampled volume. To estimate the number of pre-synaptic elements in the tissue, not just the total volume of vesicle accumulations in a given z-series, contiguous clusters of overlapped pixels larger than 0.16 μm^2 (for synaptophysin or GAD65/67 stain) or 0.10 μm^2 (for synapsin 1) were identified in the images of overlapped pixels. These sizes were previously chosen by visual inspection of stained sections to represent a conservative minimal release site size. The chosen sizes helped to eliminate accidental overlap of axons and synaptic stain and were still significantly smaller than the presynaptic specializations identified by electron microscopy in the sSC at this age (Warton and McCart, 1989). These criteria identified "puncta", presumptive pre-synaptic release sites, our indicators of a "synapse" in this report, The number of puncta in a volume was obtained using the optical disector method (Gundersen, 1986) on the overlap micrographs. Specifically, sequential z-sections were examined in 0.25 μm steps through 4 μm, and only the first incidence of each puncta was counted. Puncta appearing in the first section were not included. Optical disector analysis was possible despite the discrete z-dimension steps because the focal depth of the z-sections was approximately 30μm, which therefore leaves no unsampled region of the tissue between optical sections. We believe this method constitutes a full optical disector in accordance with *J Comp Neurol* policy.

Each volume sampled with these methods generated four measurements: (1) the volume of contralateral retinal arbors, (2) the volume of vesicle stain, (3) the number of overlapped pixels, and (4) the number of synaptic "puncta". The later two measures were normalized for the volume of retinal arbor.

All statistics used one-tailed Student's t-tests for unequal variance performed on Microsoft Excel between experimental animals and the appropriate controls. All data are reported as average ± standard error of the mean.

RESULTS

Synaptic density analysis

Synaptic contacts were visualized by immunofluorescent labeling for the vesicle-associated proteins synaptophysin or synapsin-1 in the same optical sections containing contralateral RGC axons filled with Alexa 488 fluorophore conjugated to anterograde tracer CTB. Stacks of thin optical sections acquired from 42 mm^3 volumes by laser-scanning confocal microscopy were used to identify puncta formed by the overlap of retinal axons and the antibody (Fig. 2). Synaptophysin and synapsin-1 staining was punctate and easily separable from background. Detailed analysis of synaptic distribution within contralateral retinal axons was not possible because their density prevented unambiguous following of single axons for more than a few microns (Fig. 2b,c). Examination of the lower density ipsilateral projection in the same tissue shows that the distribution of synaptophysin labeling along axons is consistent with it marking synapses; puncta are confined to en passant arbor swellings or terminal arbors (Fig. 3a). The contralateral axons appear to show the same pattern (inset Fig. 3a). The synaptophysin puncta overlapping with contralateral retinal axons ranged in size from 0.16 μm^2, the minimum size accepted, to 1.3 μm^2, the largest size detected. Average synaptophysin puncta size was 0.35 ± 0.17 μm^2. Average synapsin-1 puncta were smaller (0.24 ± 0.10 μm^2) and their minimal acceptable size was reduced accordingly (0.10 μm^2). We did not observe significant differences in puncta size between ages for either antigen. Overlapped puncta above the minimum size were identified by image analysis software, but each was subsequently examined by eye to ensure that the

synaptic stain was completely surrounded by the retinal axon before inclusion into the data set.

Sampling of the sSC was carefully designed to preclude bias by normal tissue variation in synapse density. In each animal the same regions of SGS were sampled, taking only two coronal sections at separated but consistent distances from the rostral pole, and selecting two regions at equivalent positions across the medial-lateral axis in each section (Fig. 2). Using this regime it was possible to observe significant differences from a relatively small number of animals. Synapse number was counted within each volume using an optical disector on a stack of optical sections. The number of retinal synaptic puncta was counted in four 42 mm^3 volumes from each animal (Fig. 2a). Synaptic density was determined by dividing the number of overlapped puncta counted in these volumes by the total retinal axon volume in the same volumes. A second measure of synaptic density had no minimal size criterion and was calculated as the total density of vesicle antigen within the retinal axons from each volume.

To assure that our methods had sufficient resolution to reliably exclude false overlap, we compared the pattern of axon overlap with synaptophysin reactivity or with GAD 65/67 reactivity. The former identifies all synaptic release sites while the later identifies only synapses and cell bodies of GABAergic neurons and should not overlap with the glutamate-releasing terminals in the colliculus (Fig. 3b). From each of two control animals, 6 sections caudal to those used in the study were processed for synaptophysin or GAD-65/67 antibody staining. Two volumes from each section (n=12) were used to determine the number of overlapped synaptic puncta and pixels associated with retinal terminals for each antigen. The amount of overlap that would be expected by chance was estimated by determining the overlap values after the retinal terminal images were rotated 90° The degree to which the label was greater or lower than chance was calculated by subtracting the rotated values from those determined in the non-rotated position. This “difference” value was normalized using the sum of the rotated and non-rotated values as the denominator. Positive values indicate synaptic label that is more associated with retinal terminals than would be expected by chance; label anti-associated with the axons generates a negative number (Silver and Stryker, 1999).

Image pixels containing synaptophysin were more likely to overlap with the retinal terminals than chance. The correlation coefficient was 0.40 ± 0.12 (Fig. 3c). Pixels containing GAD-65/67 antigen were anti-correlated, with a correlation coefficient of −0.36 ± 0.16 ($p<0.01$ for difference between the correlation coefficients). The overlap values, when compared using the size limited measure of puncta larger than 0.16 μm^2 overlapping the retinal axon, showed even greater differences. Overlapped synaptophysin puncta had a correlation coefficient of 0.71 ± 0.08, while the GAD puncta coefficient was −0.98 ± 0.01 ($p<0.01$). GABAergic synapses are frequently adjacent to retinal terminals in the sSC (Lund, 1969;Mize, 1988), yet we still observed only a tiny number of overlapped GAD puncta in the non-rotated condition, indicating that our imaging is of sufficient resolution to perform relative quantifications.

To document that synaptophysin puncta fully enveloped by labeled retinal axons were good indices of actual synapses, we examined their association with post-synaptic AMPA receptors. For this, separate sSC sections with contralateral axons labeled were also labeled with the synaptophysin antibody and with an antibody to one of two AMPA receptor subunits GluR1 or GluR2 (Fig. 3d). In the first triple-labeled neuropil examined, of 54 synaptophysin puncta enveloped by retinal axon label, 46 (85%) were within 0.2 μm of a GluR1 puncta. Of 49 overlapped synaptophysin puncta in a second triple labeled neuropil, 43 (88%) were within 0.2 μm of a GluR2 puncta. Many of the synaptophysin puncta not

overlapping with labeled axons failed to have an AMPAR puncta within even 1 μm, probably reflecting the fact that many sSC synapses are GABAergic(Mize, 1992). Thus, our quantitative confocal estimates of retinal axon synapse density do not appear to be seriously distorted by false overlap from inadequate resolution, image processing artifacts, or non-synaptic accumulations of vesicles within axons.

NMDAR blockade increases synaptic density

We first examined the effect of chronic blockade of NMDARs from birth by implanting thin sheets of the NMDA antagonist-infiltrated (D-AP5) or control (L-AP5-infiltrated or sham) slow release plastic Elvax above the sSC. This treatment had varying effects on the synaptic density of the contralateral retinal axons, depending upon the age of sacrifice (Table 1; Fig 5a). Animals with NMDAR blockade sacrificed on P6 and P8, during the peak period of axon terminal refinement(Simon and O'Leary, 1992), showed a 6-fold increase in synaptic density along RGC axons compared to control Elvax littermates (Fig. 4a, b). Pups examined at P10, toward the end of the refinement period, still showed increased synaptic density. However by P14, when RGC axons have developed a focused terminal projection and the pups' eyes have opened, NMDAR blockade had no significant effect on the synaptic density along RGC axons (Fig. 4d, e).

To be sure that the minimal size threshold applied for identification of synaptic puncta was not responsible for our results, total synaptophysin reactivity in retinal axons relative to the total retinal axon volume was examined. These density measures were very similar to the synaptic puncta data (Fig. 5b; Table 1): on P6 and P8 NMDAR blockade increased synaptophysin density within labeled retinal axons. At P10 and P14 there was no difference in density between NMDAR blocked and control sSC. There was no effect of NMDAR blockade on total density of synaptophysin staining in the neuropil. Our synaptic density findings were confirmed in animals killed at P8 and P14 by using an antibody against synapsin-1 instead of synaptophysin. At P8 synapsin-1 identified synaptic density was increased 7.5-fold by NMDAR blockade, while there was no apparent effect of treatment when the pups were killed at P14 (Table 1).

That NMDAR blockade increases synaptic density suggests that the dominant early effect of active NMDARs is to reduce the number of synapses that retinal axons can maintain. The absence of this blockade effect by P14 suggests that this net synaptic suppression has ended by this age, which is immediately after the completion of axonal refinement and eye opening (Simon and O'Leary, 1992). This early period when NMDAR-induced synapse elimination predominates could be terminated as a result of the increased density and refinement of the retinal and cortical projections (Lopez-Medina et al., 1989) and/or by changes in retinal and collicular activity induced by eye-opening (Yoshii et al., 2003; Liu and Constantine-Paton, 2004). To test these hypotheses small lesions of the temporal pole of the contralateral retina were made at P6. The contralateral axons that sprout into the deafferented region do so without regard to proper topography (Frost and Schneider, 1979; Simon et al., 1994), thus reinstituting conditions of axonal innervation density and topography similar to the first post-natal week. These older, sprouting axons should, when animals are killed at P14, be carrying patterns of light driven activity that are similar to normal P14 RGC axons. Therefore, by examining the synaptic density along the sprouted contralateral axons we can examine the role of axonal density as a causal factor in terminating the early period of NMDAR-induced synapse elimination. Of 45 sampled regions from 12 L-AP5 treated control pups the synaptic density along the sprouted axons was 51.44+/−10.08 synapses ($\times 10^{-3}$) per μm^3 retinal axon. The same measure from 40 regions in 10 D-AP5 treated littermates was 160.92+/−12.30 ($p < 0.01$). Thus the sprouting retinal ganglion cell axons show a response to NMDAR blockade similar to the young axons.

Synaptic depression induces synapse elimination

The early suppressive effects of NMDAR activity on RGC synapse density could reflect an active elimination of weak synapses resulting from poor activity correlations among inputs converging onto sSC neurons. If this were the case the significant anatomical reductions in RGC synapse density implied by our observation may be the structural product of NMDAR-mediated long-term synaptic depression (LTD) (Colman et al., 1997). To directly test this hypothesis we used a technique previously shown to reduce AMPAR currents in the developing sSC (Shi et al., 2001), and therefore to produce a form of chemically induced NMDAR mediated LTD (Bear and Abraham, 1996). This technique is to chronically expose the sSC to low-levels of the NMDAR agonist NMDA. NMDA-treatment begun at P8 significantly reduced synaptic density in animals killed at P14 (Fig. 4d,f; Fig. 5a; Table 1). By contrast, NMDA treatment begun at P2, before spontaneous synaptic glutamatergic currents can first be detected in the sSC slices (Shi et al., 2000), had no effect on synaptic density in animals killed at P8, during the period of peak map refinement (Fig. 4a,c; Fig. 5a; Table 1). The lack of a neonatal effect of NMDA treatment suggests that the potential for synapse elimination is normally saturated during the first postnatal week. This interpretation supports the hypothesis that during early retinocollicular development NMDARs are rarely serving in synapse stabilization. Rather, the low density and topographically unrefined nature of retinal axons means that NMDAR currents activated at their synapses almost always result in small calcium currents and synaptic depression. The total density of synaptophysin in retinal axons, irrespective of puncta size, was also reduced by NMDA treatment when the animals were killed at P14, but showed no effect at P8 (Fig. 5b; Table 1). NMDA treatment had no effect on the total synaptophysin density in the neuropil.

DISCUSSION

Effects of Early NMDAR Blockade

Our data show that NMDAR blockade increases synapse density along retinal axons during the first week and a half of postnatal life. This early effect of NMDAR blockade is not present in animals that are allowed to survive until P14 after the eyes open and afferent innervation has become dense and topographically appropriate (Lopez-Medina et al., 1989; Inoue et al., 1992; Simon and O'Leary, 1992). What causes the end of this synaptic susceptibility to NMDAR blockade is likely multifaceted. We have identified one causal factor by dennervating a small region of sSC. This causes neighboring contralateral RGC axons to sprout. On these older axons, growing within a zone of lowered innervation density and refinement, NMDAR blockade again produces an increase in synapse density. Therefore the termination of the period of NMDAR blockade-induced synaptic density is not controlled by a rigid developmental program, but is restricted by a factor requiring the increasing afferent density. The nature of this factor is not known, but could be, among others, simple synaptic density, the refinement of the projection, or physical axon-axon competition.

A synapse stabilization function has been attributed to the NMDAR during later stages of synaptic refinement (Constantine-Paton, 1990; Debski and Cline, 2002) and during cellular correlates of learning and memory (Bear and Malenka, 1994; Feldman et al., 1999). However, the current data indicate a distinctly different function for this receptor in newly innervated neuropil. During this early period, NMDAR currents could play an important role in facilitating synapse turnover and continued sorting. However, instances in which stabilization is initiated by the receptor must be rare otherwise NMDAR blockade during this period would decrease rather than increase the synaptic contacts made by contralateral retinal axons. Studies of retinotectal synaptogenesis in tadpoles and fish have advanced the idea that NMDAR function is necessary to stabilize inputs from correlated retinal ganglion

cells that are retinal neighbors (Constantine-Paton et al., 1990; Schmidt and Buzzard, 1993; Wu et al., 1996; Rajan et al., 1999a; Sin et al., 2002). Recent studies have indicated that selective branch elimination also plays a role in this refinement process (Schmidt et al., 2000; Ruthazer et al., 2003). However, no studies have actually evaluated the density of synapses made by in-growing retinal axons in newly generated tecta, or compared their normal synapse densities to densities in tecta with chronic NMDAR blockade.

Our structural evidence of a dominant NMDAR role in synapse removal in the early retinocollicular projection is fully consistent with investigations showing that long-term depression (LTD) rather than long-term potentiation (LTP) of retinocollicular synapses is present in the early rat sSC in response to robust stimulation of the optic tract (Lo and Mize, 2002; Mize and Salt, 2004). Recent work in our laboratory has shown that NMDAR-dependent LTP cannot be induced in sSC neurons until after eyes open (Zhao and Constantine-Paton, 2004). Thus the current structural data strongly support the popular hypothesis that NMDA mediated LTD represents the first stage of glutamatergic synapse removal (Stent, 1973; Bear and Rittenhouse, 1999). NMDAR-dependent limiting of synaptogenesis has been observed in hippocampal slice cultures (Luthi et al., 2001), and a similar age-dependent control of synapse density by NMDARs has been observed in the nucleus *tractus solitarii* (Vincent et al., 2004). However, these studies could not determine whether the NMDAR blockade in the source rather than target neurons was responsible for the effect, nor determine the factors that determine between synaptic elimination or stabilization. Our results suggest that NMDAR activity in the target tissue primarily results in synaptic depression and a reduction in synapse number under a limited set of circumstances that is present in early in development, as well as in cultured tissues.

Axon density and synapse elimination

The current experiments with contralateral retinal lesions suggest that factors associated with a low innervation density contribute to the period of NMDAR-dependent elimination. Further evidence for this conclusion comes from previous studies of the ipsilateral retinal projection (Colonnese and Constantine-Paton, 2001; Colonnese et al., 2005). Like the contralateral projection studies here, NMDAR blockade had no effect on the ipsilateral projection unless the innervation density was reduced by a retinal lesion. When such a lesion is performed the ipsilateral axons sprout into the dennervated region. Following NMDAR blockade these sprouting axons have a significantly higher density of synapses and a greater sprouting response. When the same eye-lesions were applied in older animals, at an age when ipsilateral axons had to compete with the late developing corticocollicular projection, NMDAR blockade had no effect. Removal of the cortex, however, reinstated the sprouting effect of the NMDAR blockade. These earlier results substantiate the conclusion of the present experiments. When innervation density is high NMDAR blockade does not induce sprouting, consistent with the hypothesis that blockade-induced increases in sprouting result because NMDAR function in neuropil with low innervation densities would otherwise produce more synapse elimination than stabilization. These experiments cannot rule out the involvement of other events such as the advent of light driven activity or changes in synaptic release, receptor composition, growth factor secretion or extracellular matrix composition as contributing factors in NMDAR effects. However, they do show that under several different conditions the NMDAR is primarily involved in eliminating retinocollciular synapses when the sSC is relatively uninnervated and the potential for strong, correlated activity is likely to be low.

Developmental switch in NMDAR function

Why, then, does NMDAR blockade have no effect after eye opening and increased afferent innervation? Our hypothesis is that these conditions cause synaptic stabilization to become

an equally prominent result of NMDAR activation at many synapses, so that by P14 the two processes are equally prominent. Therefore, when NMDARs are blocked no net change in synaptic density is observed because neither elimination nor stabilization is dominant. The conditions that increase NMDAR-mediated synaptic stabilization are likely the increasing correlation in the activity of converging afferents as a result of eye opening as well as their greater topographic refinement and innervation density. This should make the retinal axons more effective in driving NMDAR activation to the threshold needed for LTP. Evidence for the loss of NMDAR driven stabilization of synaptic contacts has been obtained after blockade in other, relatively more mature, systems. We postulate that this is due to a net increase in NMDAR-mediated stabilization at the developmental time-points used in these studies (Rajan et al., 1999a).

Alternatively, the end of the period for NMDAR-dependent synapse elimination could be brought about by changes in NMDAR function that reduce its role in structural change at retinotectal synapses. The experiments in this report involving chronic NMDA treatment of the sSC argue against this possibility. This treatment produces a profound LTD of AMPA receptor function lasting beyond the second postnatal week (Shi et al., 2001). Consequently, if NMDAR-dependent structural remodeling of mammalian retinocollicular synapses ceased around P14, this treatment should have no effect on the density of retinocollciular contacts at this age. However, we observed a pronounced decrease in contralateral RGC synapse density at P14, indicating that the NMDAR is still functioning in structural synaptic change at this older age.

The chronic NMDA treatment also provides a link between depression of particular synapses at the level of synaptic strength, and the eventual structural elimination of those synapses; such a relationship that has been proposed but not demonstrated (Bear and Rittenhouse, 1999). The reduction of synapse density by chronic NMDA application only at P14 is consistent with our hypothesis that after the early topographic refinement period ends some afferents are able to elicit a stabilizing effect through NMDAR activity. This stabilizing effect is switched back to destabilizing by the consistent induction of LTD at these synapses. That we do not see an effect of the NMDA treatment during the period of topographic refinement suggests that synaptic depression is saturated at this time; that nearly all retinal axons synapses are being eliminated and very few stabilized. This dominance of synaptic elimination during early development is not consistent with models of “metaplasticity” that posit a threshold that slides between synaptic depression and stabilization based on with recent activity (Abraham and Bear, 1996). Our results suggest that such a sliding threshold may begin only after a developmental point dependent on an increase in afferent innervation, possibly aided by the degree of correlation among neighboring RGC terminals, the onset of vision, and the makeup of the NMDAR complex.

The Role of Correlated Retinal Activity in Controlling Collicular NMDAR Function

The conclusions above raise the question: Is there evidence that retinal activity converging on the colliculus is more poorly correlated during refinement than at P14 and older? One answer is obviously yes, since the poor topographic organization of the early projection has been extensively documented (Edwards et al., 1986; O'Leary et al., 1986; Simon and O'Leary, 1990; Simon and O'Leary, 1992). With poor topography, the chances are high that poorly correlated ganglion cell inputs from distant regions of retina will converge on a single collicular neuron. However, the parameters driving RGC activity are also different. During the late fetal and neonatal periods spontaneous waves of depolarization coordinated by cholinergic amacrine cells synchronize activity in broad swatches of RGCs (Wong et al., 1993; Wong et al., 1995; Feller et al., 1996). Mice with knockouts of the β2 subunit of the nicotinic cholinergic receptor do not have correlated retinal waves early during the topographic refinement period, and consequently the RGC axon termination sites are

significantly broader in these mice than in the wild type (McLaughlin et al., 2003). Early cholinergic waves supply a level of correlated activity that allows a rough retinotopy to be established by synchronizing the activity of RGCs within hundreds of microns of each other. The waves cluster the action potentials of these neighboring RGCs within bursts, but only correlate their firing to within tens of milliseconds (Meister et al., 1991; Butts and Rokhsar, 2001). Studies of synaptic plasticity in the amphibian homologue of the sSC, the optic tectum, however, have demonstrated that spike timing on the order of *milliseconds* is critical for determining the direction of plasticity (Zhang et al., 1998).

Toward the end of the second post-natal week, light driven activity through closed or recently opened eyes will drive highly correlated spiking in neighboring rodent RGCs. This is coordinated over shorter retinal distances but within smaller time scales (Meister et al., 1995). Innervation density and point-to-point order in the projection is increasing simultaneously in the sSC (Warton and McCart, 1989). Under these conditions, tightly correlated activity capable of robustly driving the NMDAR to produce LTP should be arriving at retinocollicular synapses. In addition, with the onset of vision the composition of collicular NMDARs are changing to the mature NR2A form (Shi et al., 2000; Townsend et al., 2003; Lu and Constantine-Paton, 2004). A predominance of NR2A-containing NMDARs has been suggested to favor LTP at hippocampal synapses(Liu et al., 2004). In the sSC these changes are temporally linked with the ability to evoke NMDAR-dependent LTP of the optic fibers. Before eye opening stimulation of the afferent layer of the sSC results in LTD; however, after eye opening NMDAR-dependent LTP can be induced (Lo and Mize, 2002; Zhao and Constantine-Paton, 2004).

Significant refinement of retinofugal connectivity occurs after eye opening (Chen and Regehr, 2000; Tavazoie and Reid, 2000; Lu and Constantine-Paton, 2004). The switch in the form of NMDAR-mediated plasticity from elimination to mixed elimination and stabilization may reflect an increase in the stringency with which a distinction among afferent connections needs to be made because of the increased competition and the smaller variation in activity patterns that result from the proceeding refinement.

Technical aspects of synapse density measurements at the light microscope level

The data reported here rely on light microscope analyses of synapse density. Theoretically quantitative electron microscopic (EM) analysis of synaptic release sites, a method used previously in our lab (Yen et al., 1995), could be applied in this analysis. This might seem preferable because synaptic active sites can be identified by several criteria at the ultrastructural level. However, quantitative EM is difficult to apply to the current question because of the need to sample synapse number under a number of conditions with a low synaptic density (NMDA-treated, P6 and P8 tissue and sprouting axons). A prohibitive number of axons would need to be isolated and thoroughly filled to acquire statistically valid data under these conditions. Recently, a number of investigations have used quantitative, light microscope, techniques for assays of synapse distribution and density (Pinches and Cline, 1998; Silver and Stryker, 1999; Silver and Stryker, 2000). In dissociated culture puncta of synaptophysin reactivity associate with regions of membrane recycling indicative of active synapses (van den Pol et al., 1998; Hopf et al., 2002). Our staining for post-synaptic density proteins GluR1 and GluR2 indicate that the vast majority of the synaptophysin puncta we counted as synapses are adjacent to post-synaptic densities. Nevertheless our measures could still represent an over-estimation of synaptic density due to vesicle clusters that are not at release sites (Korkotian and Segal, 2001). For this reason the densities reported here must be treated as relative estimates between drug-treated and control neuropil, not as absolute values of retinocollicular terminal synapse density.

We have also employed the following six procedures to minimize artifacts or biases in these analyses. 1) We modified earlier light microscope methods by using the disector stereological technique, which is insensitive to changes in the shape and size of objects counted in a volume (Gundersen, 1986). Size bias is still possible in our tissue because of the minimal size criterion applied to identify synapses. We believe this is not an issue however because the minimal size used is at least one third of the average release site in the sSC at this time (Warton and McCart, 1989). Furthermore, the average puncta size did not change between treatment groups. 2) To be sure our results are not based on changes in puncta size we also used the unbiased measure of total volume of synaptic vesicle-associated immunostain in the total volume of retinal terminal, which provided similar results. 3) All analyses were treatment-blind. 4) An anti-GAD antibody was used to indicate that significant accidental overlap of nearby fluorescence is not biasing estimates of synaptic density. 5) Antibodies against two different synaptic vesicle associated proteins, synaptophysin and synapsin-1, were used to assure that results were not biased by the particular antigen/antibody interaction. Finally, 6) littermates were randomly assigned to experimental or control groups. To minimize the effects of differences between litters and tissue processing, the same processing and solutions were used for the entire litter. We should note to that the selection of sections for analysis was done by absolute, not relative distance from the rostral end of the sSC. Thus the sample from P6 and P8 rats is from a slightly more caudal region of the sSC than the older animals.

SUMMARY

This report reveals that the NMDAR is affecting synapse formation from the earliest stages of contralateral retinal innervation of the superior colliculus. During a brief developmental period, co-temporaneous with the development of retinal topography and spontaneous retinal activity, the predominant function of the NMDAR is to depress the strength of new contacts and thereby effect their elimination. This elimination likely produces synaptic turnover and facilitates further sprouting as retinal terminals deprived of one site of termination will produce more sprouts elsewhere (Sabel and Schneider, 1988). This time period when NMDAR-dependent turnover of synapses is prominent appear to be uniquely important in determining final circuit order. Fully characterizing the cellular and molecular components may allow the reactivation of synapse turnover and sorting in mature brains to allow functional recovery after trauma or disease.

Acknowledgments

This work was supported by National Institutes of Health Grant EY06039 to M. C. -P.

REFERENCES CITED

Aamodt SM, Shi J, Colonnese MT, Veras W, Constantine-Paton M. Chronic NMDA exposure accelerates development of GABAergic inhibition in the superior colliculus. J Neurophysiol. 2000; 83:1580–1591. [PubMed: 10712481]

Abraham WC, Bear MF. Metaplasticity: the plasticity of synaptic plasticity. Trends Neurosci. 1996; 19:126–130. [PubMed: 8658594]

Bansal A, Singer JH, Hwang BJ, Xu W, Beaudet A, Feller MB. Mice lacking specific nicotinic acetylcholine receptor subunits exhibit dramatically altered spontaneous activity patterns and reveal a limited role for retinal waves in forming ON and OFF circuits in the inner retina. J Neurosci. 2000; 20:7672–7681. [PubMed: 11027228]

Bear MF, Abraham WC. Long-term depression in hippocampus. Annu Rev Neurosci. 1996; 19:437–462. [PubMed: 8833450]

Bear MF, Malenka RC. Synaptic plasticity: LTP and LTD. Curr Opin Neurobiol. 1994; 4:389–399. [PubMed: 7919934]

Bear MF, Rittenhouse CD. Molecular basis for induction of ocular dominance plasticity. J Neurobiol. 1999; 41:83–91. [PubMed: 10504195]

Butts DA, Rokhsar DS. The information content of spontaneous retinal waves. J Neurosci. 2001; 21:961–973. [PubMed: 11157082]

Chen C, Regehr WG. Developmental remodeling of the retinogeniculate synapse. Neuron. 2000; 28:955–966. [PubMed: 11163279]

Cline HT, Constantine-Paton M. NMDA receptor antagonists disrupt the retinotectal topographic map. Neuron. 1989; 3:413–426. [PubMed: 2577128]

Colman H, Nabekura J, Lichtman JW. Alterations in synaptic strength preceding axon withdrawal. Science. 1997; 275:356–361. [PubMed: 8994026]

Colonnese MT, Constantine-Paton M. Chronic NMDA receptor blockade from birth increases the sprouting capacity of ipsilateral retinocollicular axons without disrupting their early segregation. J Neurosci. 2001; 21:1557–1568. [PubMed: 11222646]

Colonnese MT, Shi J, Constantine-Paton M. Chronic NMDA receptor blockade from birth delays the maturation of NMDA currents, but does not affect AMPA/kainate currents. J Neurophysiol. 2003; 89:57–68. [PubMed: 12522159]

Colonnese MT, Zhao J, Constantine-Paton M. NMDA receptor currents suppress synapse formation on sprouting axons in vivo. J Neurosci. 2005 in press.

Constantine-Paton M. NMDA receptor as a mediator of activity-dependent synaptogenesis in the developing brain. Cold Spring Harb Symp Quant Biol. 1990; 55:431–443. [PubMed: 2151924]

Constantine-Paton M, Cline HT, Debski E. Patterned activity, synaptic convergence, and the NMDA receptor in developing visual pathways. Annu Rev Neurosci. 1990; 13:129–154. [PubMed: 2183671]

Debski EA, Cline HT. Activity-dependent mapping in the retinotectal projection. Curr Opin Neurobiol. 2002; 12:93–99. [PubMed: 11861170]

Edwards MA, Schneider GE, Caviness VS Jr. Development of the crossed retinocollicular projection in the mouse. J Comp Neurol. 1986; 248:410–421. [PubMed: 3722464]

Feldheim DA, Kim YI, Bergemann AD, Frisen J, Barbacid M, Flanagan JG. Genetic analysis of ephrin-A2 and ephrin-A5 shows their requirement in multiple aspects of retinocollicular mapping. Neuron. 2000; 25:563–574. [PubMed: 10774725]

Feldman DE, Nicoll RA, Malenka RC. Synaptic plasticity at thalamocortical synapses in developing rat somatosensory cortex: LTP, LTD, and silent synapses. J Neurobiol. 1999; 41:92–101. [PubMed: 10504196]

Feller MB, Wellis DP, Stellwagen D, Werblin FS, Shatz CJ. Requirement for cholinergic synaptic transmission in the propagation of spontaneous retinal waves. Science. 1996; 272:1182–1187. [PubMed: 8638165]

Frost DO, Schneider GE. Plasticity of retinofugal projections after partial lesions of the retina in newborn Syrian hamsters. J Comp Neurol. 1979; 185:517–567. [PubMed: 438369]

Gundersen HJ. Stereology of arbitrary particles. A review of unbiased number and size estimators and the presentation of some new ones, in memory of William R. Thompson. J Microsc. 1986; 143:3–45. [PubMed: 3761363]

Hopf FW, Waters J, Mehta S, Smith SJ. Stability and plasticity of developing synapses in hippocampal neuronal cultures. J Neurosci. 2002; 22:775–781. [PubMed: 11826107]

Huang L, Pallas SL. NMDA antagonists in the superior colliculus prevent developmental plasticity but not visual transmission or map compression. J Neurophysiol. 2001; 86:1179–1194. [PubMed: 11535668]

Inoue K, Terashima T, Inoue Y. Postnatal development of the corticotectal projection from the visual cortex of the mouse. Okajimas Folia Anat Jpn. 1992; 68:319–331. [PubMed: 1603524]

Korkotian E, Segal M. Regulation of dendritic spine motility in cultured hippocampal neurons. J Neurosci. 2001; 21:6115–6124. [PubMed: 11487635]

Liu L, Wong TP, Pozza MF, Lingenhoehl K, Wang Y, Sheng M, Auberson YP, Wang YT. Role of NMDA receptor subtypes in governing the direction of hippocampal synaptic plasticity. Science. 2004; 304:1021–1024. [PubMed: 15143284]

Lo FS, Mize RR. Properties of LTD and LTP of retinocollicular synaptic transmission in the developing rat superior colliculus. Eur J Neurosci. 2002; 15:1421–1432. [PubMed: 12028352]

Lopez-Medina A, Bueno-Lopez JL, Reblet C. Postnatal development of the occipito-tectal pathway in the rat. Int J Dev Biol. 1989; 33:277–286. [PubMed: 2641348]

Lu W, Constantine-Paton M. Eye opening rapidly induces synaptic potentiation and refinement. Neuron. 2004; 43:237–249. [PubMed: 15260959]

Lund RD. Synaptic patterns of the superficial layers of the superior colliculus of the rat. J Comp Neurol. 1969; 135:179–208. [PubMed: 4181001]

Luthi A, Schwyzer L, Mateos JM, Gahwiler BH, McKinney RA. NMDA receptor activation limits the number of synaptic connections during hippocampal development. Nat Neurosci. 2001; 4:1102–1107. [PubMed: 11687815]

McLaughlin T, Torborg CL, Feller MB, O'Leary DD. Retinotopic map refinement requires spontaneous retinal waves during a brief critical period of development. Neuron. 2003; 40:1147–1160. [PubMed: 14687549]

Meister M, Lagnado L, Baylor DA. Concerted signaling by retinal ganglion cells. Science. 1995; 270:1207–1210. [PubMed: 7502047]

Meister M, Wong RO, Baylor DA, Shatz CJ. Synchronous bursts of action potentials in ganglion cells of the developing mammalian retina. Science. 1991; 252:939–943. [PubMed: 2035024]

Mize RR. Immunocytochemical localization of gamma-aminobutyric acid (GABA) in the cat superior colliculus. J Comp Neurol. 1988; 276:169–187. [PubMed: 3220979]

Mize RR. The organization of GABAergic neurons in the mammalian superior colliculus. Prog Brain Res. 1992; 90:219–248. [PubMed: 1321459]

Mize RR, Salt TE. Contribution of GABAergic inhibition to synaptic responses and LTD early in postnatal development in the rat superior colliculus. Eur J Neurosci. 2004; 20:1331–1340. [PubMed: 15341604]

O'Leary DD, Cowan WM. Topographic organization of certain tectal afferent and efferent connections can develop normally in the absence of retinal input. Proc Natl Acad Sci U S A. 1983; 80:6131–6135. [PubMed: 6193529]

O'Leary DD, Fawcett JW, Cowan WM. Topographic targeting errors in the retinocollicular projection and their elimination by selective ganglion cell death. J Neurosci. 1986; 6:3692–3705. [PubMed: 3794796]

O'Leary DD, Yates PA, McLaughlin T. Molecular development of sensory maps: representing sights and smells in the brain. Cell. 1999; 96:255–269. [PubMed: 9988220]

Pinches EM, Cline HT. Distribution of synaptic vesicle proteins within single retinotectal axons of Xenopus tadpoles. J Neurobiol. 1998; 35:426–434. [PubMed: 9624623]

Rajan I, Witte S, Cline HT. NMDA receptor activity stabilizes presynaptic retinotectal axons and postsynaptic optic tectal cell dendrites in vivo. J Neurobiol. 1999a; 38:357–368. [PubMed: 10022578]

Rajan I, Witte S, Cline HT. NMDA receptor activity stabilizes presynaptic retinotectal axons and postsynaptic optic tectal cell dendrites in vivo. J Neurobiol. 1999b; 38:357–368. [PubMed: 10022578]

Ruthazer ES, Akerman CJ, Cline HT. Control of axon branch dynamics by correlated activity in vivo. Science. 2003; 301:66–70. [PubMed: 12843386]

Sabel BA, Schneider GE. The principle of "conservation of total axonal arborizations": massive compensatory sprouting in the hamster subcortical visual system after early tectal lesions. Exp Brain Res. 1988; 73:505–518. [PubMed: 3224660]

Schmidt JT, Buzzard M. Activity-driven sharpening of the retinotectal projection in goldfish: development under stroboscopic illumination prevents sharpening. J Neurobiol. 1993; 24:384–399. [PubMed: 7684064]

Schmidt JT, Buzzard M, Borress R, Dhillon S. MK801 increases retinotectal arbor size in developing zebrafish without affecting kinetics of branch elimination and addition. J Neurobiol. 2000; 42:303–314. [PubMed: 10645970]

Shi J, Aamodt SM, Constantine-Paton M. Temporal correlations between functional and molecular changes in NMDA receptors and GABA neurotransmission in the superior colliculus. J Neurosci. 1997; 17:6264–6276. [PubMed: 9236237]

Shi J, Aamodt SM, Townsend M, Constantine-Paton M. Developmental depression of glutamate neurotransmission by chronic low-level activation of NMDA receptors. J Neurosci. 2001

Shi J, Townsend M, Constantine-Paton M. Activity-dependent induction of tonic calcineurin activity mediates a rapid developmental downregulation of NMDA receptor currents. Neuron. 2000; 28:103–114. [PubMed: 11086987]

Silver MA, Stryker MP. Synaptic density in geniculocortical afferents remains constant after monocular deprivation in the cat. J Neurosci. 1999; 19:10829–10842. [PubMed: 10594065]

Silver MA, Stryker MP. A method for measuring colocalization of presynaptic markers with anatomically labeled axons using double label immunofluorescence and confocal microscopy. J Neurosci Methods. 2000; 94:205–215. [PubMed: 10661840]

Simon DK, O'Leary DD. Limited topographic specificity in the targeting and branching of mammalian retinal axons. Dev Biol. 1990; 137:125–134. [PubMed: 1688537]

Simon DK, O'Leary DD. Development of topographic order in the mammalian retinocollicular projection. J Neurosci. 1992; 12:1212–1232. [PubMed: 1313491]

Simon DK, Prusky GT, O'Leary DD, Constantine-Paton M. N-methyl-D-aspartate receptor antagonists disrupt the formation of a mammalian neural map. Proc Natl Acad Sci U S A. 1992; 89:10593–10597. [PubMed: 1359542]

Simon DK, Roskies AL, O'Leary DD. Plasticity in the development of topographic order in the mammalian retinocollicular projection. Dev Biol. 1994; 162:384–393. [PubMed: 8150202]

Sin WC, Haas K, Ruthazer ES, Cline HT. Dendrite growth increased by visual activity requires NMDA receptor and Rho GTPases. Nature. 2002; 419:475–480. [PubMed: 12368855]

Smith AL, Cordery PM, Thompson ID. Manufacture and release characteristics of Elvax polymers containing glutamate receptor antagonists. J Neurosci Methods. 1995; 60:211–217. [PubMed: 8544481]

Stent GS. A physiological mechanism for Hebb's postulate of learning. Proc Natl Acad Sci USA. 1973; 70:997–1001. [PubMed: 4352227]

Tavazoie SF, Reid RC. Diverse receptive fields in the lateral geniculate nucleus during thalamocortical development. Nat Neurosci. 2000; 3:608–616. [PubMed: 10816318]

Townsend M, Liu Y, Constantine-Paton M. Retina-driven dephosphorylation of the NR2A subunit correlates with faster NMDA receptor kinetics at developing retinocollicular synapses. J Neurosci. 2004; 24:11098–11107. [PubMed: 15590926]

Townsend M, Yoshii A, Mishina M, Constantine-Paton M. Developmental loss of miniature N-methyl-D-aspartate receptor currents in NR2A knockout mice. Proc Natl Acad Sci U S A. 2003; 100:1340–1345. [PubMed: 12552130]

van den Pol AN, Obrietan K, Belousov AB, Yang Y, Heller HC. Early synaptogenesis in vitro: role of axon target distance. J Comp Neurol. 1998; 399:541–560. [PubMed: 9741482]

Vincent A, Kessler JP, Baude A, Dipasquale E, Tell F. N-methyl-d-aspartate receptor activation exerts a dual control on postnatal development of nucleus tractus solitarii neurons in vivo. Neuroscience. 2004; 126:185–194. [PubMed: 15145084]

Warton SS, McCart R. Synaptogenesis in the stratum griseum superficiale of the rat superior colliculus. Synapse. 1989; 3:136–148. [PubMed: 2928962]

Wong RO, Chernjavsky A, Smith SJ, Shatz CJ. Early functional neural networks in the developing retina. Nature. 1995; 374:716–718. [PubMed: 7715725]

Wong RO, Meister M, Shatz CJ. Transient period of correlated bursting activity during development of the mammalian retina. Neuron. 1993; 11:923–938. [PubMed: 8240814]

Wong WT, Myhr KL, Miller ED, Wong RO. Developmental changes in the neurotransmitter regulation of correlated spontaneous retinal activity. J Neurosci. 2000; 20:351–360. [PubMed: 10627612]

Wu G, Malinow R, Cline HT. Maturation of a central glutamatergic synapse. Science. 1996; 274:972–976. [PubMed: 8875937]

Yen L, Sibley JT, Constantine-Paton M. Analysis of synaptic distribution within single retinal axonal arbors after chronic NMDA treatment. J Neurosci. 1995; 15:4712–4725. [PubMed: 7540683]

Zhang LI, Tao HW, Holt CE, Harris WA, Poo M. A critical window for cooperation and competition among developing retinotectal synapses. Nature. 1998; 395:37–44. [PubMed: 9738497]

Zhao J, Constantine-Paton M. Chronic NMDA treatment and suceptibility to NMDA mediated potentiation in the developing superior colliculus. 2002 Abrstract Viewer/Itinerary Planner. 2002 331.336.

Zhao, J.; Constantine-Paton, M. 2004 Abstract Viewer/Itinerary Planner. Washington, DC: Society for Neuroscience, 2004; 2004. Eye opening changes plastcity at visual synapses. Online. Program No. 154.11

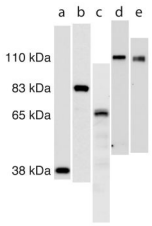

Figure 1. Antibodies used for immunohistochemistry recognize a single band in juvenile superior colliculus

Western blots from 4–14% poly-acrylamide gels after running denatured, whole lysate of the superficial visual layers of superior colliculus of P14 rats. The scans of lanes have been approximately aligned to show the relative kDa of bands. The lanes are as follows: (a) synaptophysin, (b) synapsin-1, (c) GAD 65/67, (d) GluR1, (e) GluR2. The GAD 65/67 antibody recognizes a doublet as expected, while the others recognize a single band as can be seen in the figure that includes the entire length of each lane.

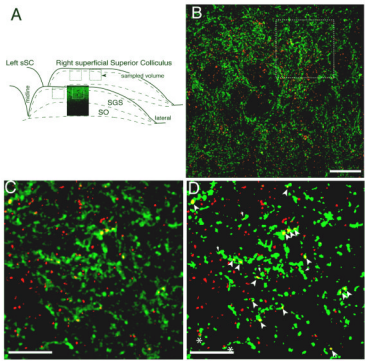

Figure 2. Counting of retinal ganglion cell axon synapses

Synapses were identified by immunolabeling for synaptophysin combined with anterograde tracing of the contralateral retinal projection using fluorescently tagged cholera toxin. A. Sampling scheme. A confocal micrograph of the contralateral retinal projection (green) is shown inset into a schematic of the sampled field within the sSC. B. A typical optical section of a sampled sSC field. Contralateral retinal axons are green; synaptophysin labeling is red. Synaptic density counting was performed on a stack of such sections from a 4 μm-deep volume. The outlines of cell bodies and blood vessels are seen as distinct areas of low synapse density. C. Detail showing the distribution of axons and synaptophysin stain and the pattern of overlap (yellow). D. A binary image of C created with the threshold protocol used for the synaptic density analysis (see Methods). Puncta formed by the overlap of the label larger the 0.16μm^2 and completely engulfed by the axon (large arrowheads) were counted as synapses. Smaller puncta (small arrowheads) and partial overlap (asterisk) were not counted. Scale bars 20 μm, 10μm.

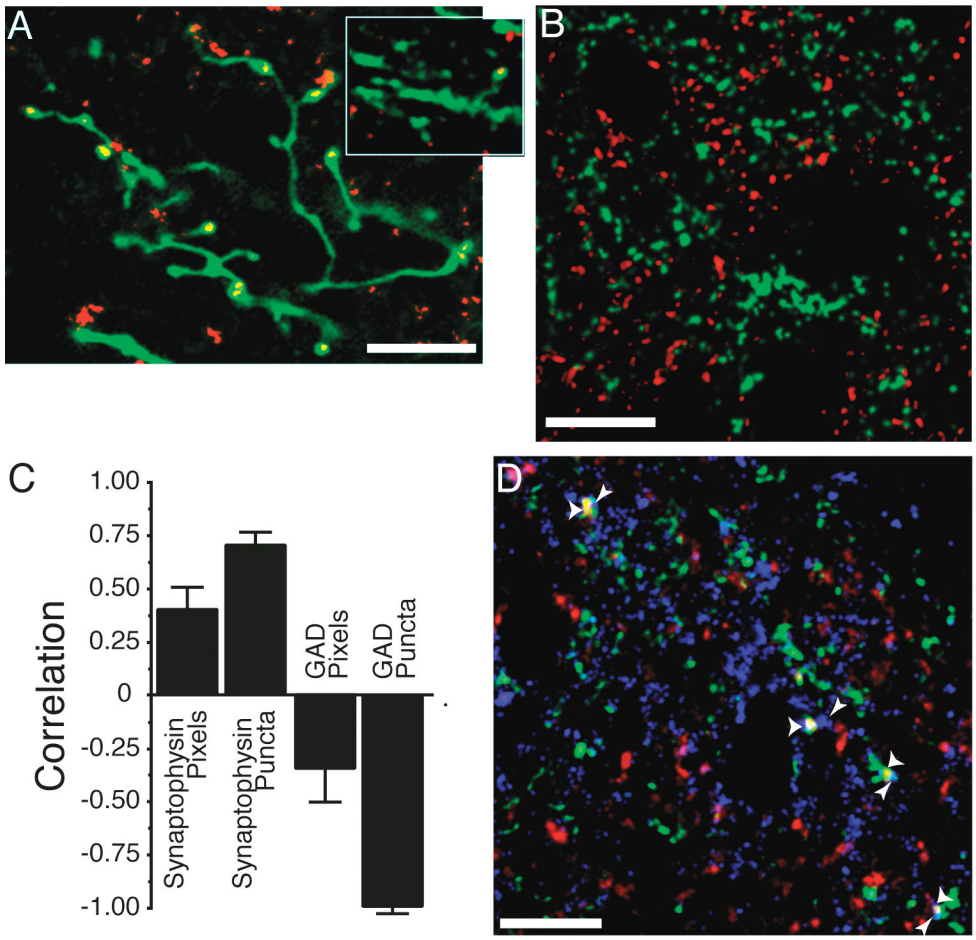

Figure 3. Immunohistochemistry for synapse associated proteins can be used to count retinal ganglion cell axon synapses

A. The pattern of synaptophysin staining within an axon is consistent with its identity as a synapse. The image is a collapsed confocal z-series from a 10 μm depth of tissue. Synaptophysin puncta occur in expansions of the axon either at terminal points or *en passant*. This image was taken within the stratum opticum of the ipsilateral colliculus where the axonal caliber is larger and synaptic density is lower. This allows for reconstruction over greater depths to visualize the entire arbor without interference from other axons. Other images presented in this paper are single confocal sections, which is required because of the density of contralateral axons in the SGS (for example, Fig. 2). A single confocal section from the contralateral retinal projection zone that contains a portion of arbor is shown in the inset. The localization of synaptophysin is similar to that seen in the ipsilateral projection, where the exact localization can be better ascertained. B. Sample confocal micrograph showing double labeling of retinal axons (green) and GAD 65/67 (red). Unlike the synaptophysin double labeling (Fig. 2B), there was no overlap between the two labels here. Even though our antibody recognizes GAD 65 and GAD 67, the majority of staining was restricted to processes with only light staining of cell bodies, indicating that GAD 65 was primarily localized during these overlap experiments. C. Correlation coefficients of overlap between ipsi axons and the immunostain for synaptophysin or GAD 65/67. The GAD stain is used as a control because it should never co-localize with retinal axons. Positive correlation indicates that the overlap of axon and antigen is greater than would be expected

by chance (see Methods). This correlation coefficient was determined for the total number of overlapped “Pixels”, as well as for the number of pixel accumulations that exceeded 0.16 μm^2 (“Puncta”), our minimal criterion for a synapse. Synaptophysin antigens show more overlap, and GAD-65/67 localization shows less overlap, than would be expected by chance, especially when the minimal size criterion is imposed. Data for each antigen were acquired from 12 sections from two animals. D. Overlapped synaptophysin puncta are adjacent to post-synaptic markers. A confocal micrograph of tissue triple labeled for the ipsilateral RGC axons (green), synaptophysin (red – overlap is yellow), and also for the post-synaptic glutamate receptor GluR1 (blue). Presumptive synapses are marked with wide arrowheads. All identified presumptive synapses are adjacent to at least one GluR1 puncta that does not overlap with the retinal axon (thin arrowheads). Scale bars 10 μm.

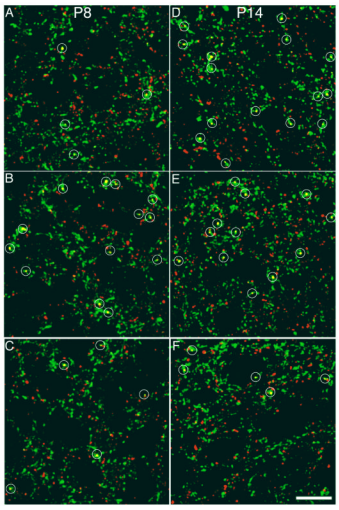

Figure 4. NMDA receptor activity regulates synaptic density on contralateral retinal axons in an age dependent manner

Sample confocal micrographs of the SGS from various ages and treatment groups that show contralateral retinal axons (green) and synaptophysin label (red). Regions of overlap (yellow) that met the criteria for synapses are marked by a white circle. Drug treatment was provided by the slow release plastic Elvax in which an NMDAR antagonist (D-AP5), an agonist (NMDA) or an appropriate control (L-AP5 or water) was infused. Pups were killed during the period of retinotopic map refinement (P8) or after eye opening and map-refinement (P14). The panels are from the following treatment groups. A. P8 Control, four synapses; B. P8 NMDAR antagonist-treated, thirteen synapses; C. P8 NMDAR agonist-treated, four synapses; D. P14 Control, fifteen synapses; E. P14 NMDAR antagonist-treated, twelve synapses; F. P14 NMDAR agonist-treated, five synapses. Scale bar 10 μm.

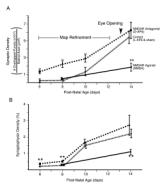

Figure 5. NMDA receptor activity suppresses synapse formation during the period of retinocollicular map refinement

The average and standard error of RGC axon synaptic density for two experimental treatments--(1)NMDAR antagonist (D-AP5) treated (red) and (2) NMDAR agonist-treated (green)--and (3) the grouped controls are plotted. The control littermates from each of these experiments (L-AP5 and sham Elvax, respectively) have been grouped. NMDAR blockade increased synaptic density when animals were killed on P6, P8 or P10 but not P14. Conversely, agonist-treatment, known to functionally depress synapses, reduced densities at P14 but not P8. That NMDAR blockade increases synaptic density during the period of topographic refinement suggests that at this time the receptor is functioning to actively reduce synapse number on RGC axons. B. A second analysis of the same images to determine total density of synaptophysin staining within the retinal axons. This analysis shows our results are not dependent on the minimum size criterion for puncta, but that total synaptophysin density is regulated in a manner similar to synaptic density. Double asterisk indicates significant difference ($p<0.01$) from the age-matched, treatment-specific control group.

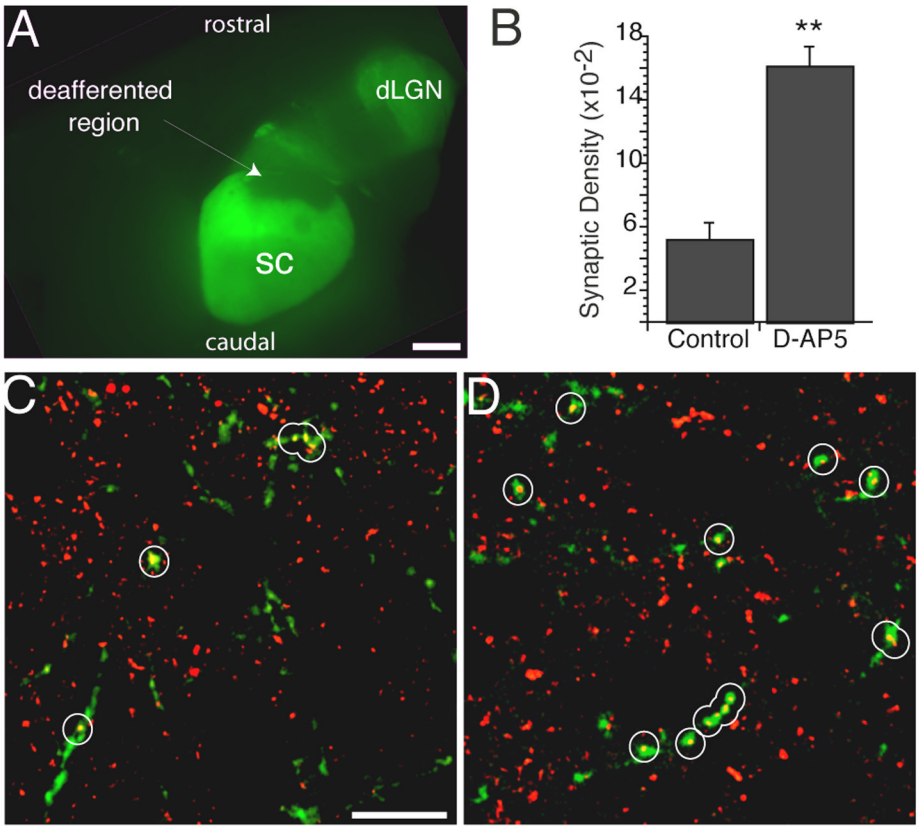

Figure 6. Decreased axonal density allows NMDAR blockade to increase synaptic density

A. A small lesion of the temporal retina deafferents a region of the rostral sSC. This is shown here in a whole mount of the mid and forebrain with cortex removed. The retinal projection from the lesioned eye has been labeled with a green fluorescent tracer. The scotoma can be seen in the whole mount by lack of green staining. Lesions were made at P6 and the animals sacrificed at P14. Under these conditions, axons from the remaining ganglion cells sprout into the deafferented region. B. Synaptic density, measured as described in Figure 1 and Figure 3 for control and NMDAR blocked (D-AP5) littermates, is increased by NMDAR blockade along the sprouting axons inside the deafferented region. C. Sprouted axons are of lower density, but can be examined for synapses as in the unlesioned projection. Shown here is a high power confocal micrograph taken within the deafferented region of a control pup in a manner the same as described in Figure 1. The retinal axons are green; synaptophysin stain is red. Synapses are marked with white circles. D. Similar image from within the deafferented region of an NMDAR antagonist treated pup. Synapses density is higher along the retinal axons. ** $p < 0.01$. Scale bars 1mm, 10 μm.

Table 1

Synaptic Density and total antigen overlap are tabulated by antibody and by age in post-natal days (P). Population averages are plus or minus standard error of the mean. Number of animals constituting the average for each group is given under 'n'. Averages were derived from four volumes from each rat. Significant difference from control by Student's t-test is demarcated by asterisk

	Conrol		NMDAR blocked		Control		NMDA Agonist	
AGE	**L-AP5**	**(n)**	**D-AP5**	**(n)**	**Sham**	**(n)**	**NMDA**	**(n)**
SYNAPTOPHSYIN SYNAPSE DENSITY ((synapses per μm^3) × 10^{-3})								
P6	2.61 +/− 0.44	(7)	13.03 +/− 2.31**	(8)				
P8	3.19 +/− 0.61	(8)	22.21 +/− 3.94**	(8)	3.90 +/− 0.77	(9)	4.87 +/− 1.23	(8)
P10	13.21 +/− 5.07	(6)	28.87 +/− 4.33**	(7)				
P14	68.93 +/− 11.98	(8)	54.21 +/− 7.37	(7)	58.16 +/− 12.17	(7)	18.59 +/− 4.72**	(7)
SYNAPTOPHYSIN PIXEL DENSITY ((overlapped pixels/total axon pixels) ×10^{-3})								
P6	2.16 +/− 0.34	(7)	3.73 +/− 0.51**	(8)				
P8	2.36 +/− 0.21	(8)	5.21 +/− 0.60**	(8)	3.27 +/− 0.66	(9)	3.05 +/− 0.59	(8)
P10	15.07 +/− 2.00	(6)	16.64 +/− 2.11	(7)				
P14	24.39 +/− 5.21	(8)	27.24 +/− 6.10	(7)	20.02 +/− 2.28	(7)	11.00 +/− 1.63**	(7)
SYNAPSIN-1 SYNAPSE DENSITY ((synapses per µm3) ×10^{-3})								
P8	1.09 +/− 0.16	(8)	7.57 +/− 1.00**	(8)				
P14	29.42 +/− 6.90	(8)	31 +/− 5.58	(7)				
SYNAPSIN-1 PIXEL DENSITY ((overlapped pixels/total axon pixels) ×10^{-3})								
P8	0.59 +/− 0.29	(8)	4.82 +/− 1.36*	(8)				
P14	20.08 +/− 7.22	(8)	25.37 +/− 6.77	(8)				
LESION SYNAPSE DENSITY ((synapses per μm^3) ×10^{-3})								
P14	51.22 +/− 10.08	(12)	160.92 +/− 12.30**	(10)				

* $p < 0.05$

** $p < 0.01$